



Original article

Identifying priority heat-risk areas in Granada, Spain, using InVEST and landscape metrics

Carson Silveira^{a,b} , Nuria Pistón^{a,c,*} , Javier Martínez-López^{a,c} ,
Domingo Alcaraz-Segura^{a,d,e} , Thedmer Postma^a, Juan M. López-Torralbo^f,
Regino Zamora^{a,c} 

^a Interuniversity Institute of Earth System Research in Andalusia (IISTA), University of Granada, Av. del Mediterráneo s/n, Granada 18071, Spain

^b Programa de Pós-graduação em Ecologia, Universidade Federal do Rio de Janeiro, Av. Carlos Chagas Filho, 373, Rio de Janeiro, RJ 21941-590, Brazil

^c Dept. of Ecology, University of Granada, Av. Fuentenueva s/n, Granada 18071, Spain

^d Dept. of Botany, University of Granada, Av. Fuentenueva s/n, Granada 18071, Spain

^e Andalusian Center for Global Change (ENGLoba), University of Almería, Crta. Sacramento s/n, Almería 04120, Spain

^f The Environmental Hydraulics Institute (IH Cantabria), C. Isabel Torres, 15, Santander 39011, Spain

ARTICLE INFO

Keywords:

Adaptation

Ecosystem services

Green infrastructure

InVEST

Landscape metrics

Urban heat island

ABSTRACT

The urban heat island effect and its disproportionate impact on vulnerable groups is a major challenge for cities. The aim of this research is to identify heat-risk areas and to examine the effect of vegetation spatial patterns on heat mitigation. The focus of the study is on Granada, Spain, and its metropolitan area, serving as a relevant case study due to its status as a medium-sized city within the Mediterranean region, a location particularly vulnerable to climate change. We used InVEST for urban heat island modelling and calculated heat vulnerability and exposure indices. We also used Boosted Regression Trees to assess the importance of the spatial composition and configuration of the vegetation in heat mitigation. We identify priority heat-risk areas for intervention highlighting regions where high heat exposure and vulnerability overlap. Our results show that the combination of green cover above 35 % and mean patch size above 200 m² maximized heat mitigation. However, because most of the priority areas are located in densely populated and built-up areas, the suggested approach could be on creating interconnections between smaller green infrastructures to increase their cooling capacity. We highlight the need for urban planning strategies that prioritize heat-vulnerable populations, while optimizing the spatial configuration of green infrastructure by focusing on Nature-based Solutions.

1. Introduction

How urbanization affects the climate is a well-known topic in scientific literature and its effects on rising temperatures have been well documented (Oke, 1973; Arnfield, 2003; Chakraborty and Qian, 2024). The Urban Heat Island (UHI), where urban areas are significantly warmer than the countryside, is one of the most visible aspects of human impacts and many studies have explored its formation, magnitude, configuration, consequences and evolution (Peng et al., 2012; Liu et al., 2022; Ren et al., 2023; Chakraborty and Qian, 2024). UHI results from the use of surfaces and materials that are impermeable and with low albedo, which reduce evaporation rate and local evapotranspiration, altering the radiative balance leading to more heat in urban areas (Oke, 1973; Arnfield, 2003). In addition to impermeability and the materials

used in urban areas, UHI is related to anthropogenic heat, pollution and the structure and surface roughness of cities, which can, for example, alter wind flow and facilitate heat retention (Armfield, 2003). The UHI operates at different scales (Ren et al., 2023; Chakraborty and Qian, 2024), being correlated with health problems and ecological changes (Kleerekoper et al., 2012; De Pauw et al., 2024; Jungman et al., 2023) and worsened by circumstances that are the result of social injustice in the cities (Jenerette et al., 2011; Rocha et al., 2024).

Higher temperatures in cities put the resident's quality of life at risk due to heat extremes, which tend to worsen (Coffel et al., 2017; Tuholske et al., 2021) along with the intensification of the current climate crisis scenario, which is projected to particularly increase severe extreme events in urban areas (Peng et al., 2012; Li and Bou-Zeid, 2013). Heat stress is already one of the major climate-related causes of human

* Corresponding author at: Dept. of Ecology, University of Granada, Av. Fuentenueva s/n, Granada 18071, Spain.

E-mail address: nuriapiston@ugr.es (N. Pistón).

<https://doi.org/10.1016/j.ufug.2025.128794>

Received 19 December 2024; Received in revised form 17 March 2025; Accepted 20 March 2025

Available online 23 March 2025

1618-8667/© 2025 Elsevier GmbH. All rights are reserved, including those for text and data mining, AI training, and similar technologies.

premature death in Europe (Romanello et al., 2023), and with heat-waves becoming more severe and prolonged, more people is expected to be at risk in the future (Perkins et al., 2012; Russo and Domeisen, 2023). Health injuries caused by prolonged exposure to high temperatures ranges from heat exhaustion, heatstroke, and cardiovascular and respiratory diseases (Hess et al., 2023; Romanello et al., 2023). However, despite a general increase in heat exposure worldwide, this phenomenon does not occur homogeneously (Tuholske et al., 2021). Some demographic groups are disproportionately more affected by high temperatures and considered vulnerable, including the elderly, children, low-income communities, and outdoor workers who often lack access to adequate cooling mechanisms (Schwartz, 2005; Aldrich and Benson, 2007). Furthermore, urban areas with less tree cover and fewer green spaces, which tend to be the most economically disadvantaged areas of the city (e.g. Jiao et al., 2021; Pistón et al., 2022), experience intensified UHI effects, compounding social inequalities in heat exposure and health outcomes. Thus, the intersectionality of socioeconomic, racial, age and gender factors add to vulnerability due to the higher risk of exposure, highlighting the importance of assessing patterns of heat risk to foster locally tailored adaptation strategies (Chakraborty et al., 2019; Prosdocimi and Klima, 2020; Hsu et al., 2021; Chen et al., 2023; Mashhoodi and Kasraian, 2024).

The Fifth Assessment of the IPCC adopted a framework to assess heat risks as a function of vulnerability, exposure and hazard (see Oppenheimer et al., 2014). Recent studies have used this approach to map and explore the relationship of heat impacts with demographic variables (Chakraborty et al., 2019; Hsu et al., 2021; Chen et al., 2023). However, while these studies provide crucial insights into heat vulnerability, they often overlook the role of urban morphology and land cover characteristics in shaping localized heat exposure (Marando et al., 2022). Furthermore, most research does not usually address the intrinsic relationship between the cooling benefits provided by green infrastructures (GI includes forest, parks, gardens, street trees), and the effects of heat exposure (Zhou et al., 2021; Iungman et al., 2023; Georgescu et al., 2024). Recent investigations at fine-scale spatial resolution stand out as promising for mitigating risks to the population, like addressing inequalities in access to urban natural spaces in Shaoxing (Zhou, Chen & Xu, 2022), investigating how to optimize the implementation of green roofs in high-density urban areas in Xiamen Island (Dong et al., 2024) or assessing heat exposure variation through time in US cities (Georgescu et al., 2024). Given that one of the strategies most suggested is increasing green infrastructure in cities as a Nature-based Solution (Iungman et al., 2023), the search for understanding the relationship between green infrastructures and heat risk locally could be an important way of using more effective and equitable adaptive strategies to reduce the risk (Iungman et al., 2023).

While increasing the percentage of green cover is consistently linked to temperature reduction, the spatial arrangement of GI can significantly influence their cooling impact (Li et al., 2011; Chen et al., 2014a,b; Kong et al., 2014). For example, in over 90 European cities, increasing tree coverage to 30 % has been shown to result in a temperature decline of 0.4 °C on average and to prevent more than 2000 premature deaths during summer (Iungman et al., 2023). A growing body of literature has shown that GI effects on temperature stem from different climatic conditions, scale of analysis, and ecological context, along with the interaction between all these factors, resulting in a synergistic but variable influence of landscape configuration (i.e. green cover and how it's distributed) on temperature reduction (Zhou et al., 2011; Li et al., 2013; Li and Bou-Zeid, 2013; Silveira et al., 2024). However, most studies are still conducted at the city level in Northern Europe, the United States or Asia, (e.g., Bosch et al., 2021; Hamel et al., 2024; Kadaverugu et al., 2021; Zawadzka et al., 2021). Despite these advancements, there is a critical gap in research focusing on Mediterranean cities, where dense urbanization and limited space for GI implementation require further attention. Addressing these gaps through high-resolution data and spatially explicit models can provide more tailored insights for cities

struggling with limited space for new green infrastructure (Marando et al., 2022; Massaro et al., 2023). The effect of landscape structure and the organization of GI on temperature mitigation could be considerably more important in such densely packed cities, where the possibilities for increasing green infrastructure and other Nature-based Solutions can be challenging (Haaland and van den Bosch, 2015; Delgado-Capel and Cariñanos, 2020).

This study applied a framework to identify heat-risk areas and assess spatial vegetation patterns that will maximize heat mitigation using high-resolution data and a spatially explicit model. Our main hypothesis was that vegetation distribution is a determining factor in the mitigation of the urban heat island. First, we focus on one of the regions most threatened by desertification in Europe (i.e., Mediterranean region; Mirzabaev et al., 2019) where studies are still scarce. Second, we widen the lens from the city focus to the metropolitan area, while maintaining a very fine spatial scale (2 m) to obtain highly precise results on heat exposure and vulnerability hotspots that can be further translated into actions. Thus, using the metropolitan area of Granada, Spain, as a case study, this work aimed to map and evaluate heat risk indices. Using biophysical data, like shade, crop coefficient, temperature, evapotranspiration and land use and land cover, we modelled the urban heat island and calculated heat vulnerability and exposure indices to assess the distribution and degree of people's exposure and vulnerability to heat, using the results of the InVEST urban cooling model, a widely used model (Bosch et al., 2021; Hamel et al., 2024; Kadaverugu et al., 2021; Zawadzka et al., 2021). We also quantified the relationship between vegetation spatial patterns and heat mitigation using Boosted Regression Trees. Identifying priority heat-risk exposure and vulnerability areas, along with the optimal vegetation patterns to maximize cooling, is crucial for urban stakeholders to prioritize areas for developing climate adaptation and resilience strategies.

2. Methods

2.1. Study area

We considered the city of Granada as an excellent model because: 1) it is in the Mediterranean basin, a place where climate impact is particularly evident, 2) it is one of the Spanish cities with the highest levels of atmospheric pollution, 3) it is a city with a medium-sized urban area (about 200,000 inhabitants), surrounded by a belt of nearby towns that approximately accumulate the same amount of population, forming a metropolitan area of a size and structure very similar to many other cities in the world. Specifically, the study includes municipalities within the "plan for urban agglomeration of Granada" that we will call the "La Vega de Granada Belt", in southern Spain. La Vega de Granada Belt is located at the foot of the Sierra Nevada, in a vast flood plain and close to the Mediterranean coast. The study area includes 31 municipalities in addition to the city of Granada itself. Since 1975, Granada (680 m.a.s.l.) has been among the Spanish cities most affected by heat waves (Delgado-Capel et al., 2023). The region has an altitude range up to 3100 m and a transitional climate between cold semi-arid climate (Bsk) and the Mediterranean (Csa) due to its proximity to the coast and to the vast mountain system of Sierra Nevada (Hidalgo-García and Arco-Díaz, 2022).

2.2. InVEST urban cooling model

The Integrated Valuation of Ecosystem Services and Tradeoffs software (InVEST) provides spatially explicit models suitable to study ecosystem services supply and their impact on our quality of life. Specifically, the spatial distribution of heat islands is modelled based on the land use and land cover (LULC) of location (Natural Capital Project, 2024). The InVEST urban cooling model was designed and created as an open-source tool to aid urban management and planning, adapted to different data availability contexts, being able to spatially estimate air

temperature through computer simulations (Hamel et al., 2021). In addition to simplifying the assessment, with the urban cooling model it is possible to evaluate the cooling capacity and evaluate scenarios with different land use arrangements, which can directly help to assess, for example, the effects of different green zone implementation strategies. InVEST urban cooling model has been proposed as an alternative to those models that require many parameters and are complex to use (Hamel et al., 2021), however, there are still few studies evaluating its performance (Bosch et al., 2021; Hamel et al., 2024; Kadaverugu et al., 2021; Zawadzka et al., 2021), as well as extending the application of its results to the construction of heat risk indices as a tool to aid city decision-making. The model considers both local cooling contributions and the influence of larger urban parks that extend their cooling effects beyond their boundaries. It builds upon the methodology for estimating the cooling capacity (CC; Eq. 1) of green infrastructure, in accordance with Zardo et al. (2017), while incorporating additional parameters such as albedo:

$$CC_i = 0.6 \times shade + 0.2 \times albedo + 0.2 \times ET_i \quad (1)$$

CC is calculated by weighting three factors: shading, albedo and evapotranspiration, the mechanisms used by vegetation to reduce its surrounding temperature and regulate the radiative balance (Phelan et al., 2015; Zardo et al., 2017; Natural Capital Project, 2024). Shading represents tree canopy contributions, with values assigned based on tree height (>2 m). Albedo captures surface reflectivity, where higher values indicate greater solar reflectance and reduced heat absorption. ET_i (as in Eq. 2) is derived as the ratio of reference evapotranspiration (ETO) to the maximum evapotranspiration (ETO_{max}) within the area, where ETO accounts for land cover-specific evapotranspiration using crop coefficients.

$$ET_i = kc \times ETO / ETO_{max} \quad (2)$$

To incorporate the heat mitigation effect of large green areas (>2 ha) on those surrounding them, the model calculates the Heat Mitigation Index (HMI). For pixels that are not affected by large green areas, HMI is equivalent to CC. For pixels within the influence zone of large green areas, the HMI is determined as a distance-weighted average ($dcool$) of the cooling values of the green areas and the pixel, reflecting the attenuation of cooling effects with distance. The model estimates land use and cover effects on air temperature using LULC data and biophysical data (Table 1). To estimate heat mitigation, the model incorporates the urban heat island magnitude. The air temperature (Eq. 3) for each pixel without mixing is calculated as:

$$Tair_{nomix} = Tair_{ref} + (1 - HMI) \times UHImax \quad (3)$$

where the reference temperature is $Tair_{ref}$, and the maximum UHI effect is $UHImax$, defined as the difference between $Tair_{ref}$ and the highest observed temperature in the city. The modelled air temperature, accounting for mixing $Tair$, is derived from $Tair_{nomix}$ by applying a Gaussian smoothing function.

The InVEST urban cooling model is an open-source tool for urban management and planning which is used to spatially estimate air temperature through computer simulations (Hamel et al., 2021). The cooling capacity of different land use arrangements and scenarios can be assessed helping to predict the impacts of different green zone implementation strategies. It serves as an alternative to models that require many parameters and are complex to use (Hamel et al., 2021). However, there are still a few studies evaluating its performance (Bosch et al., 2021; Hamel et al., 2024; Kadaverugu et al., 2021; Zawadzka et al., 2021), as well as the suitability of its results as a trustworthy tool to support city decision-making.

2.2.1. Model input variables and parameters

The InVEST urban cooling model requires three sets of inputs: a land cover map, a table of biophysical properties, and rasters of climatic

Table 1

Summary of the datasets and parameters used in our study with their respective references from which data was retrieved. The names of datasets and parameters follow the nomenclature provided by the InVEST Urban Cooling Model (see Natural Capital Project, 2024). All data used in this work are available in Silveira et al. (2025).

Dataset	Description	Source	Resolution
SIPNA Land use and Land Cover *	SIPNA Land Use and Land Cover vector map of 2020 for the study area	Sistema de Información sobre el Patrimonio Natural de Andalucía (SIPNA) (REDIAM, 2023a) Instituto Geográfico Nacional (2023)	1:10000
Buildings*	The 2023 Base Topográfica Nacional de España vector dataset to extract buildings to build the LULC raster	Plan Nacional de Ortofotografía Aérea (PNOA, 2020a)	1:2000
Vegetation*	2020–2021 RGBIr orthophotography to derive green infrastructure to build the LULC raster	Plan Nacional de Ortofotografía Aérea (PNOA, 2020b)	0.25 m/ pixel
Height*	LiDAR point-cloud dataset for 2020 to assign height values to buildings and vegetation classes to build the LULC raster	Google Earth Engine	0.5 point/ m
LST	Raster of Land Surface Temperature mean values for 2020 retrieved from Landsat 8 TIR bands	REDIAM (2023b)	30 m
ETO	Raster map of mean reference evapotranspiration values for 2020	Agencia Española de Meteorología (AEMET) (https://opendata.aemet.es/centrodedescargas/inicio)	500 m/ pixel
Tref	Average air temperature for 2020 in a non-urban reference area (where urban heat island effect is not observed)	Red del Servicio de Calidad Ambiental (CMAOT)	-
UHImax	Magnitude of the heat island. It was obtained from the difference between highest average temperature from climatological station record and Tref	Allen et al. (1998); Grimmond & Oke (1999)	-
Kc*	Crop coefficient; indicates the evapotranspiration rate for plant organisms	Zawadzka et al. (2021)	-
Green area* *	Indicates whether or not a LULC class is considered a green area (1 or 0)	Zawadzka et al. (2021)	-
Shade* *	Proportion of tree vegetation cover (at least 2 m high)	Taha et al. (1988)	-
Albedo* *	Proportion of solar radiation that is reflected by a surface.	Natural Capital Project (2024)	-
dcool	Cooling Distance. Distance in meters where GI greater than 2 ha has a cooling effect	Natural Capital Project (2024)	-
r	Air mixing radius in meters	Natural Capital Project (2024)	-
Relative weight	Shade, evapotranspiration and albedo parameters relative weight values applied while calculating the cooling capacity index.	Natural Capital Project (2024)	-
Population density	Number of people per census tract in 2020	Instituto de Estadística y Cartografía de Andalucía (2020a)	-
Elderly population	Proportion of people > 65 per census tract in 2020	Instituto de Estadística y	-

(continued on next page)

Table 1 (continued)

Dataset	Description	Source	Resolution
Medical facilities	Number of medical facilities, disregarding dental clinics for 2023	Cartografía de Andalucía (2020a) Instituto de Estadística y Cartografía de Andalucía (2020b)	-
Income	Average family income per census tract in 2020	Instituto Nacional de Estadística (2020a)	-
Poverty	Class of households with an income of less than 60 % per census tract in 2020	Instituto Nacional de Estadística (2020b)	-

* Datasets used to build final LULC raster map to run InVEST Urban Cooling Model.

** Values presented in the biophysical table and corresponding to each LULC class.

variables (Natural Capital Project, 2024). In this work, we built the LULC raster required for the calculation of the HMI by fusing four different datasets in QGIS 3.16 software (see Table 1): i) the 2020 SIPNA land use and land cover vector dataset (scale 1:10000; REDIAM, 2023a) to differentiate the built-up, crop, and non-crop vegetation classes from other classes; ii) the 2023 Base Topográfica Nacional de España vector dataset (scale 1:2000; Instituto Geográfico Nacional, 2023) to extract buildings; iii) the 2020 RGBI orthophotography (0.25 m/pixel; PNOA, 2020a) to derive green infrastructure (i.e., vegetation) and, iv) the 2020 LiDAR point-cloud dataset (0.5 points/m; PNOA, 2020b) to assign height values to buildings and vegetation classes. In this study, the NDVI was computed from Eq. (4), with NIR and R being spectral radiance measurements in Near Infrared and red regions, respectively. Height outliers such as undesired returns from birds, dust or other elements, or sensor errors were removed using LAStools v180520. The combination of LiDAR and NDVI data allowed us to differentiate the green infrastructure into two classes: tree and shrub-herbaceous.

$$NDVI = \frac{NIR + red}{NIR - red} \quad (4)$$

For the biophysical table (Table 2), each LULC class was assigned values of evapotranspiration coefficient (Kc), albedo, and shading, as well as if it was considered as green infrastructure or not. The Kc assigned to each LULC class was approximated from existing studies on evapotranspiration for different vegetation types and on evaporation for building areas (Allen et al., 1998; Grimmond and Oke, 1999). We obtained albedo values from Taha et al. (1988), and shading variables and green areas were based on the considerations of Zawadzka et al. (2021), which includes vegetation and water bodies as green areas.

Lastly, the urban cooling model requires the potential evapotranspiration raster and temperature data to calculate the cooling effects and simulate air temperature. We used 2020 evapotranspiration raster

Table 2

Biophysical data referring to land use and land cover classes. The "green area" column describes whether the class will be considered (1) or not (0) as a green area. Kc refers to the crop coefficient value to each LULC class. The albedo column describes the proportion of solar radiation associated with each LULC class.

LULC code	LULC classes	Shade	Kc	Albedo	Green Area
1	Grass/Shrubs	0	1	0.18	1
2	Trees	1	0.97	0.16	1
3	Build-up	0	0.25	0.14	0
4	Wetlands	0	0.65	0.09	0
5	Bare and sparse vegetation	0	0.4	0.30	0
6	Buildings	0	0.01	0.20	0
7	Tree crops	1	1.4	0.20	1
8	Croplands	0	1.45	0.20	1

derived from the Thornwhite method (500 m/pixel, REDIAM, 2023b). This raster served as an input for the InVEST, quantifying the cooling effect of vegetation via evapotranspirative processes. For reference temperature (Tref), we used the annual mean temperature for the year 2020 in the Granada airport weather station (Agencia Estatal de, 2023), a reference area outside the city with no urban heat island effect, as recommended by Hidalgo-García and Arco-Díaz (2022). UHImax was calculated with the difference between Tref and mean annual temperature of a weather station in the central urban area of Granada (Red del Servicio de Calidad Ambiental-CMAOT, 2020) (Fig. 1). All data used in this work are available in Silveira et al. (2025).

2.2.2. InVEST validation

Validation is a crucial step in assessing the reliability of models, especially as their use for decision-making grows. Despite InVEST widespread application, few studies have validated the urban cooling model (Bosch et al., 2021; Hamel et al., 2024; Kadoverugu et al., 2021; Zawadzka et al., 2021), limiting our understanding of its applicability across different urban contexts. Increasing validation efforts can help refine the model's assumptions and improve its predictive capabilities. Furthermore, the validation process is a crucial step not only for ensuring the robustness of our results but also for guiding the selection of the most appropriate InVEST air temperature output for the subsequent heat risk index analyses conducted in this work.

To validate our urban cooling model, we performed a Pearson correlation analysis at two levels: grid resolution (raster pixels) and census tract level, the latter representing a scale pertinent to urban management and policy decision-making. For grid resolution we have compared the 2 m/pixel air temperature output grid from InVEST and the monthly mean Land Surface Temperature (LST) values in 2020 at 30 m resolution, retrieved from Landsat 8 imagery obtained from Google Earth Engine. For a fair comparison, we followed Zawadzka et al. (2020; 2021) and reproduced for the air temperature output grid the processing using Landsat 8 TIR bands at 100 m resolution, but then resampled to 30 m/pixel. Thus, our first step was to upscale the 2 m InVEST results to 100 m and then downscale them to the final 30 m resolution to be comparable with the LST. For the census tract-level analysis, we aggregated both the InVEST-modeled air temperature and the LST values by averaging the data within each census tract. This aggregation allowed us to compare the temperature estimates at a scale relevant to urban planning and decision-making (Zawadzka et al., 2021). After transforming the data to the same resolution, an overall validation was performed using Pearson correlation to test the relationship between the air temperature model results and the LST temperature values for all levels. Additionally, we calculated heat indices based on the InVEST-modeled temperature (HEinvest) and LST (HELst) and tested their correlation. Finally, we conducted a Moran's I analysis to evaluate spatial autocorrelation in the results.

2.3. Heat Indexes and heat-risk areas

We focus on heat risk integrating exposure, vulnerability, sensitivity, and adaptability. We have followed the framework proposed by globally recognized reports from the IPCC, 2012 and ESPON Climate, 2022, as well as other case studies like Wang et al. (2023) and Ye and Yang (2025). Thus, we ensure consistency and which allows for an overall comparison. Heat Vulnerability (HV) is related to sensitivity and adaptability, and it measures "the propensity of a person or group that influences their ability to anticipate, cope with, resist and recover from the adverse effects of physical events" (IPCC, 2012). HV is calculated by the following formula (Eq. 5):

$$HV = S - A \quad (5)$$

Where S is sensitivity and A is adaptability. HV values were normalised ranging from 0 to 1, using the maximum difference normalisation

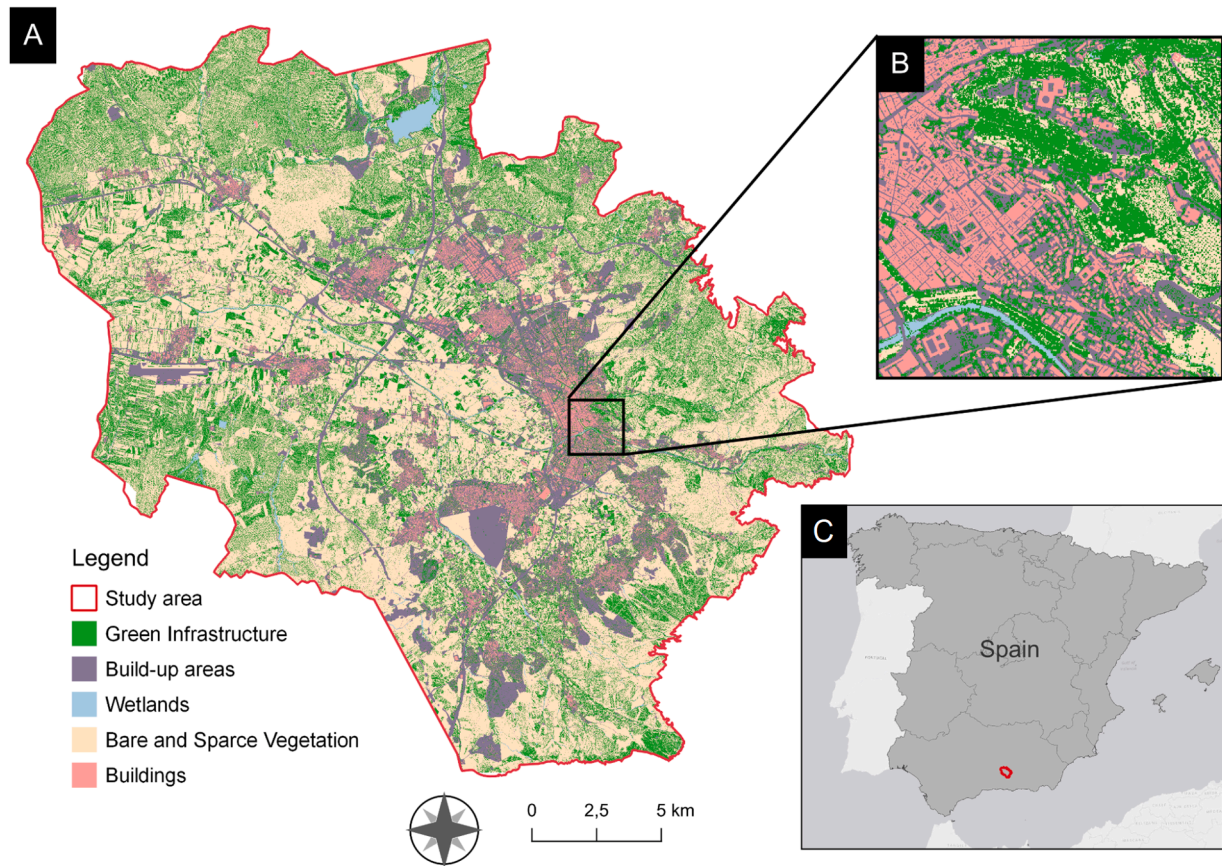


Fig. 1. Land use/land cover map (LULC) showing the LULC used in the modeling (A). Detail of the land use classes (B) and the location of the Granada metropolitan area (C).

method, and then categorised into five levels, i.e., very low (0–0.2), low (0.2–0.4), moderate (0.4–0.6), high (0.6–0.8) and very high (0.8–1). Adaptability (A) means "the potential of a system or population to modify its features and behavior so as to better cope with existing and anticipated stresses" (IPCC, 2012) and is measured as the availability of medical resources and household income (Eq. 6):

$$A = 0.5Z(\text{med}) + 0.5Z(\text{income}) \quad (6)$$

Where the number of medical facilities is $Z(\text{med})$, the household income is $Z(\text{income})$ and 0.5 is the predefined multiplication factor. The other component of HV, Sensitivity (S), is understood as "the capacity to be harmed by extreme heat in terms of one's health and physical well-being" (IPCC, 2012). S depends on the proportion of the population aged over 65 (> 65) and a measure of poverty (Eq. 7):

$$S = 0.5y(\text{elderly}) + 0.5y(\text{poverty}) \quad (7)$$

Where $y(\text{elderly})$, is the proportion of persons aged > 65 , and $y(\text{poverty})$ is the class of households living below 60 % of the poverty threshold. 0.5 is a predefined multiplication factor used by Wang et al. (2023).

Furthermore, to assess the rate of population that inherently are exposed to heat, we calculated the Heat Exposure (HE) index, meaning "the presence of people that were exposed in high temperature and thereby could suffer adverse impact by heat" (IPCC, 2012). This index can be described by the equation (Eq. 8):

$$HE = 0.5 \times (po) + 0.5x(t) \quad (8)$$

The HE index is a function of population density $x(po)$ and temperature, $x(t)$. To validate InVEST air temperature results, we calculated HE using two types of temperature: air modelled temperature by InVEST (HEinvest) and LST (HELst).

Finally, we assessed the results generated by the InVEST model and its applicability for mapping priority heat-risk areas. Priority areas are considered targets for future intervention and were defined as the areas where the most vulnerable and heat-exposed populations are located. These priority areas were identified based on overlapping the 25 % upper quartile values for heat vulnerability and both, HEinvest and HELst (Herreros-Cantis et al., 2024). All the data used to calculate the indexes were gathered from the sources detailed in Table 1.

2.4. The influence of green infrastructure spatial patterns on heat mitigation

To assess the role of the spatial configuration and landscape structure of green infrastructure on the mitigation of the heat island effect, six landscape metrics were assessed. These metrics are usually categorized as: configuration metrics, which characterize their spatial arrangement (e.g., mean patch area, patch density, number of patches, clumpiness, and edge density) and composition metrics, which quantify the abundance of specific landscape elements (e.g., percentage of vegetation cover; Table 3). These metrics were selected for their ability to capture the distribution, fragmentation, size, and coverage of the green infrastructure, as well as for their widespread use, interpretability, and low redundancy (Zhou et al., 2011; Wang et al., 2014; Chen et al., 2014a). We calculated the metrics using the *landscapemetrics* package (Hesselbarth et al., 2019) in R v. 4.3.3.

To evaluate the influence of landscape metrics and their combined effects on heat mitigation, we employed Boosted Regression Trees (BRTs), a method that combines regression trees with a boosting technique to enhance predictive accuracy. BRTs offer several advantages, such as identifying key variables, handling nonlinear relationships and interactions, and accommodating various explanatory variables without

Table 3

Landscape metrics used to study the effects of green infrastructure (GI) spatial patterns on heat mitigation.

Categories	Landscape metrics	Description	Unit
Composition	Green cover	Proportion of the GI per sampling unit	%
Configuration	Mean patch area	The average area of GI per sampling unit	ha
	Patch density	The number of GI per 100 ha per sampling unit	GI/ha
	Edge density	Total perimeter of GI per ha per sampling unit	m/ha
	Number of patches	Total number of GI per sampling unit	n
	Clumpiness	Measure of organization of the GI in relation to the aggregation of fragments. Ranges from -1 (disaggregated) to +1 (aggregated)	-

needing data transformation or outlier removal (Elith et al., 2008). We used heat mitigation as the response variable and landscape metrics as explanatory variables. BRT's strength lies in its capacity to capture interactions based on tree size by sequentially summing numerous regression trees (Elith et al., 2008). We fixed tree complexity (tc) to 20, to test the improvement of the model's predictive capacity, and tested different combinations of bag fraction (bf), learning rate (lr) and step size during the model's parametrization process. These parameters determine the contribution of each tree, the data added at each stage, the number of trees that are generated, and the amount of nodes per tree (Elith et al., 2008). Selection for bf , lr , and step size parameters is based on the greatest explained deviation and at least 1000 trees (Table S1). We then iteratively calibrated tc , testing values from 1 to 20, running 100 simulations for each tc value to estimate confidence intervals. The model's predictive power was measured by the R^2 and the significance of the explanatory variables. We averaged the 100 R^2 values to assess model performance and estimate the relative importance of predictors (Pistón et al., 2019). The selection of the optimal tc value was done using an ANOVA with R^2 as the response variable and tc as the explanatory variable. Optimum tc was identified as first values not significantly different from subsequent values, indicating a performance plateau (Pistón et al., 2019). We also used the optimal tc and the function *gbm.interactions* to assess if interactions among explanatory variables were modelled. To interpret the bivariate relationship between heat mitigation and the predictor variables, Partial Dependence Plots were used. The full BRT methodology is described in Pistón et al. (2019). Analyses were conducted with the *dismo* (Hijmans et al., 2017) and *multcomp* packages (Hothorn et al., 2008) in R v. 4.3.3.

3. Results

3.1. Urban cooling model validation

A positive relationship was found between modelled air temperature and LST that varied from weak to moderate, depending on whether the relationship was tested on a pixel-by-pixel basis or aggregated by census tract (with r values between 0.21 and 0.45; Fig. S1). The highest correlation coefficient was observed in the relationship between LST and modelled air temperature that included air mixing, which accounts for the influence of wind in redistributing heat and reducing temperature variability ($r = 0.45$; Fig. S1a).

3.2. Patterns of heat vulnerability and exposure

We found a high degree of heterogeneity in the distribution of HV in our study area with highest levels occurring in the city center and north and south parts of Granada and the north of Armilla city, with most census tracts (42 %) showing intermediate values of vulnerability (Fig. 2A). For HELst and HEinvest, the two indices showed a very narrow distribution of values, with most census tracts showing intermediate values of heat exposure for the study area (around 40 % for HEinvest and 46 % for HELst). Nevertheless, for both indices, there is a spatial concentration of higher heat exposure values in the central region of the study area, equivalent to the urban core of the city of Granada (Fig. 2B; 2C).

We found a significant and high correlation between HELst and HEinvest ($r = 0.85$; Fig. S2). Spatially, using the Moran's I index, the results show a significant and highly similar cluster formation for both HELst and HEinvest, that is, clusters with high values of HE tend to be surrounded by other clusters with high HE values (Fig. S3). We found a tendency for greater exposure in the central region of Granada, where the old town and the highest population density is located, forming a high exposure cluster. There are also cluster regions of low temperature around Granada, far from the central area. In both cases, clusters with a very similar spatial distribution for extreme values are identified, even though the HEinvest appears to overestimate all clusters, which can be attributed to the simplistic way in which the model considers the effect of air mixing.

3.3. Identification of priority areas for implementing heat mitigation strategies

Both HELst and HEinvest yield very similar results identifying around 10 % of the study area as priority areas for heat mitigation (Fig. 3; Fig. S4). This result highlights the overlap between the most vulnerable populations and those most exposed to heat in the metropolitan area of

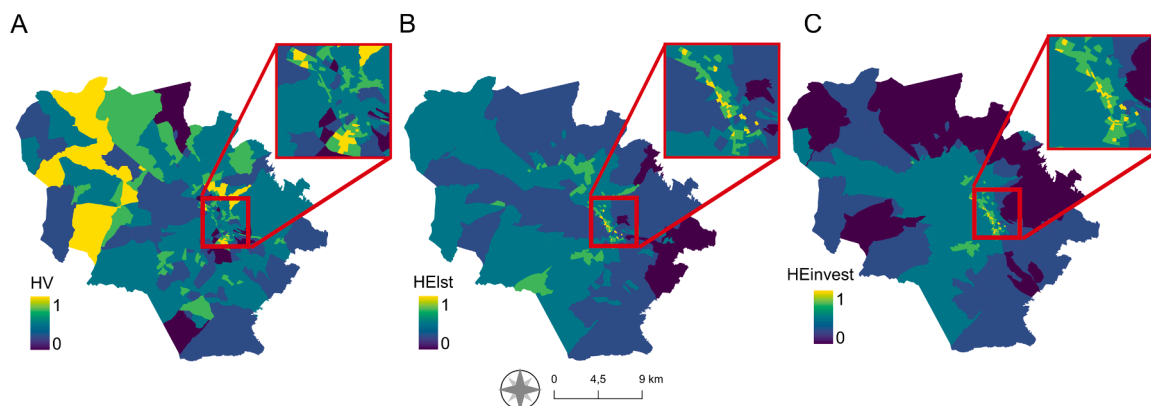


Fig. 2. Spatial distribution of (A) heat vulnerability, (B) heat exposure calculated with land surface temperature (HELst) and, (C) heat exposure calculated with InVEST air modeled temperature (HEinvest). Area inside the red square panels shows the urban core area of the city of Granada.

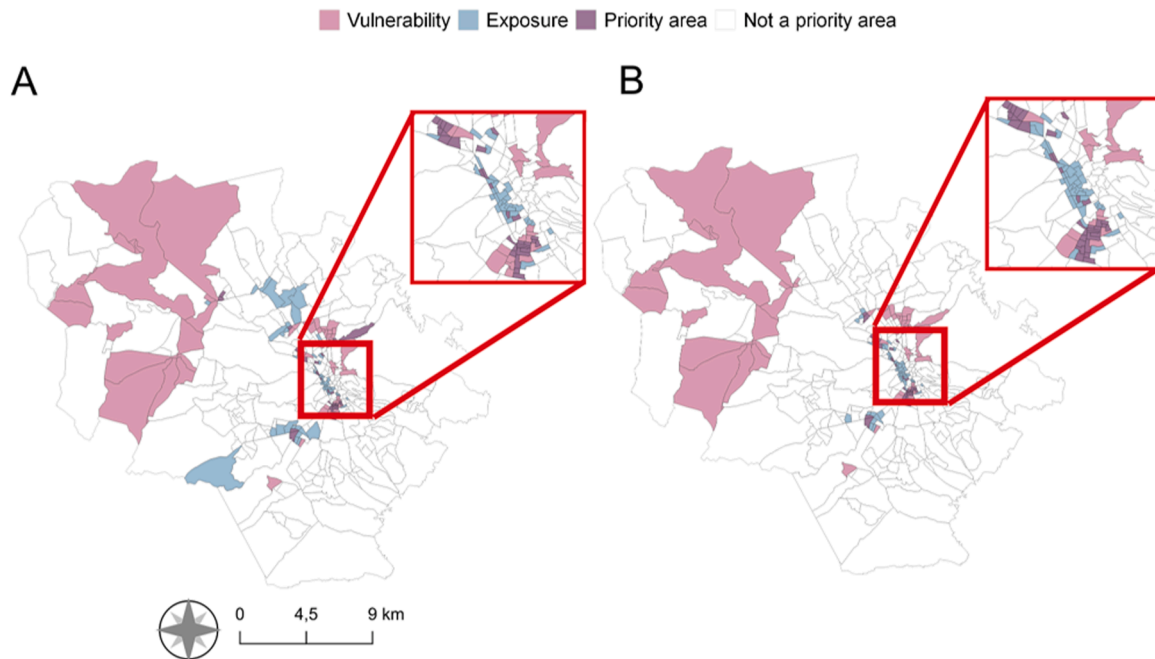


Fig. 3. Map of priority areas for heat mitigation strategies. Exposed, vulnerable and priority areas calculated with land surface temperature (LST) (A) and exposed, vulnerable and priority areas calculated with modeled air temperature from InVEST (B). Colored areas were defined based on the selection of top (25 %) quartiles across the study area. Area inside the red square panels shows the urban core area of the city of Granada, where the majority of priority areas were identified.

Granada. In particular, four main regions could be defined as priority areas for heat mitigation strategies with three being inside Granada city, i.e., part of the south and north area and the city center, and one outside, the north of Armilla city. Other areas have only high vulnerability or high exposure (Fig. 3; Fig. S4).

3.4. The combined effect of green cover and mean patch area maximizes heat mitigation

To assess the role of vegetation composition and configuration for heat mitigation (Fig. S5), we first selected the BRT model parameters, i.e., $lr = 0.001$; $bf = 0.75$, step size = 0.50 and $tc = 14$ (Table S1; Fig. S6). BRT results showed that the proportion of green cover was the most important predictor of heat mitigation (90.7 % of relative influence; Fig. 4). However, we found a combined effect of percentage of green cover with both, mean patch area, and patch density on heat mitigation (Fig. 5; Table S2), showing that the higher the green cover, mean patch area and patch density the greater the heat mitigation. The results of the Partial Dependence Plots showed that, specially both, we need to take into account a minimum green cover and green patch area to maximize the cooling capacity of vegetation in the metropolitan area of Granada. Although green cover may be the most influential factor, the spatial arrangement of vegetation (such as patch size) might still offer valuable insights in specific scenarios. Thus, the maximization was reached with green cover greater than approximately 35 % and mean area of green patches higher than 200 m² (Fig. S7). Heat mitigation did not show a large variation with edge density, the number of patches, patch density and clumpiness, being also the predictors with less relative influence on cooling capacity.

4. Discussion

We employed the INVEST urban cooling model to identify both heat-risk areas with high vulnerability and exposure in the Granada metropolitan area and the vegetation spatial patterns that maximize heat mitigation. The findings from this study emphasize the complexity of Urban Heat Island (UHI) mitigation and the challenges presented by

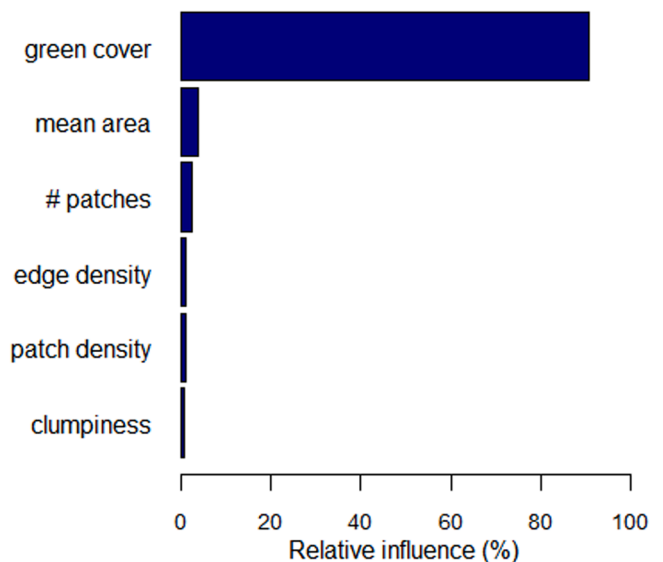


Fig. 4. Heat mitigation is mostly explained by the percentage cover of green area. The relative influence was calculated by averaging 100 simulations for the optimal value of tree complexity ($tc = 14$) using Boosted Regression Trees. Heat mitigation was considered as the response variable and landscape metrics as explanatory variables.

vulnerability and exposure to heat in urban areas. Our research highlights the importance of exploring biophysical and social data to provide a deeper understanding of heat risk in cities, focusing on Mediterranean regions. However, we need to consider some important aspects when applying the InVEST urban cooling model to assess green infrastructure's impact on heat mitigation. The model's reliance on a simplified linear relationship between tree cover and temperature reduction may not accurately reflect the complex, non-linear interactions observed in empirical studies (Ziter et al., 2019; Silveira et al., 2024). Additionally, the Mediterranean climate is characterized by hot,

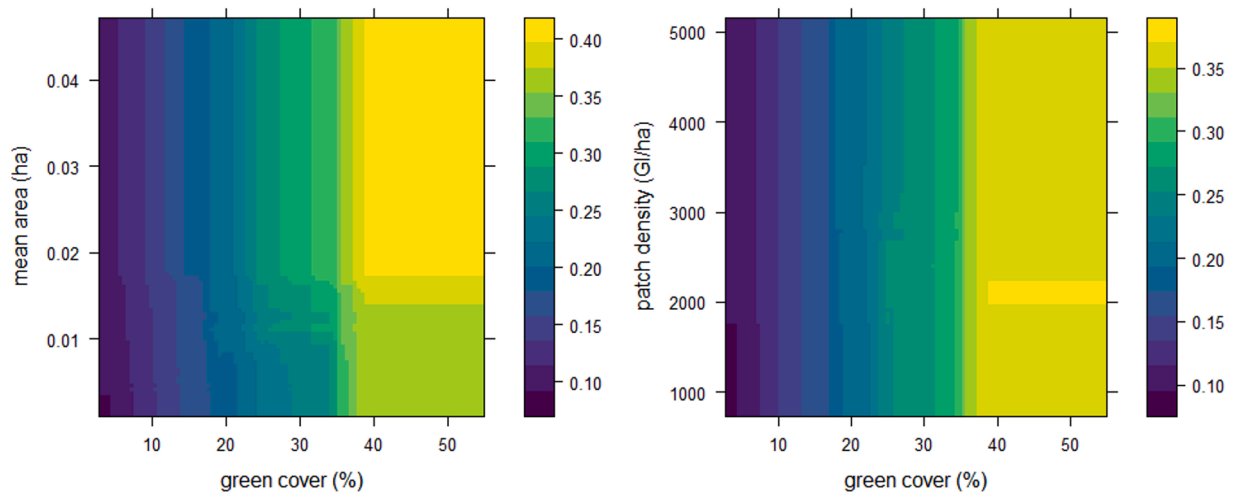


Fig. 5. Interaction plot between green cover and patch mean area (left panel) and green cover and patch density (right panel). The color bar indicates brighter and darker tones representing high and low adjusted values for heat mitigation, respectively. The maximization of heat mitigation was reached with the percentage of green cover greater than approximately 35 % and mean area of patches higher than 200 m². Patch density did not have a relevant effect.

dry summers and mild, wet winters, leading to significant seasonal variations in the urban heat island (UHI) effect (Hidalgo-García and Arco-Díaz, 2022; Delgado-Capel et al., 2023). We used the 500 m resolution Thornthwaite's evapotranspiration raster data as it was readily available. However, there may be alternative evapotranspiration methods more suitable for our study area such as the Penman-Monteith method, although these tend to be more complex and labor-intensive. Future studies should use other evapotranspiration methods and data with more refined resolution that could offer more precise estimates, while balancing model complexity and data availability. Our focus on average annual temperatures may overlook these seasonal dynamics, potentially underestimating the seasonal effectiveness of green infrastructure. To address this, future studies could incorporate data from multiple seasons in the model to capture a more accurate representation of the heat mitigation process throughout the year, particularly during the dry and hot summers. Moreover, the model does not fully account for the specific vegetation types and water requirements suited to arid conditions prevalent in Mediterranean regions, which are crucial for sustainable green infrastructure planning (Shashua-Bar et al., 2011). Therefore, incorporating local climate characteristics, seasonal variations, and appropriate vegetation selection into the model is essential to enhance its applicability and accuracy in Mediterranean urban areas.

The relationship between LST and air temperature observed at a broader spatial scale is in line with the results of other studies that have validated the InVEST urban cooling model in different cities. (Coutts et al., 2016; Hamel et al., 2024; Kadaverugu et al., 2021; Zawadzka et al., 2021). The moderate correlation between LST and InVEST average air temperature can be partially attributed to the inherent differences between the two datasets. The lack of sufficient meteorological station data in the study region rendered this comparison unavoidable, and it should be noted that discrepancies could be expected. Despite that, it is important to highlight that the model was still able to identify nearly identical areas of vulnerability when compared with LST data. This alignment demonstrates the model's effectiveness in identifying priority areas at the spatial scale used in our study.

Moreover, the strong correlation between Heat Exposure calculated with modelled air temperature and LST ($r = 0.82$), supports the applicability of the InVEST urban cooling model to identify priority areas for heat-related intervention (Hamel et al., 2024; Silveira et al., 2024; Zawadzka et al., 2021). While the diurnal urban cooling model has inherent limitations in simulating absolute air temperatures (Hamel et al., 2024; Zawadzka et al., 2021), our validation confirms its reliability in capturing spatial patterns of heat exposure. These findings

underscore InVEST's broader applicability across diverse urban contexts, positioning it as a valuable tool for city management and governance. Furthermore, our results highlight its potential to inform and support the widespread implementation of nature-based solutions and heat adaptation strategies, contributing to more climate-resilient urban environments.

Our results show that in the metropolitan area of Granada, vulnerable groups, including elderly and low-income groups, are more likely to be exposed to higher levels of heat, a finding that is consistent with previous studies that emphasize the disproportionate impact of climate risks on marginalized groups (Chakraborty et al., 2019; Hsu et al., 2021). Addressing such social inequalities should be a priority in city management and climate adaptation strategies. The identification of priority areas for heat-risk mitigation is consistent with studies that highlight densely populated, urbanized areas as UHI hotspots (Peng et al., 2012; Kleerekoper et al., 2012). These regions, which are characterized by both high heat vulnerability and high heat exposure, should be the focus of urban policies aimed at mitigating and adapting to the UHI effect. Green infrastructure, including parks, forests and urban and peri-urban agricultural areas, has been consistently cited as a key adaptation strategy (Iungman et al., 2023; Prado et al., 2024; Zhou et al., 2022). Our findings reinforce this idea, demonstrating that green cover, particularly when greater than 35 %, and mean patch size above 200 m², is a critical factor in heat mitigation (as shown in Fig. 5). Interestingly, our results show a weak but significant negative relationship between vulnerability and heat mitigation, indicating that the most vulnerable areas also have the lowest amount of green infrastructure to mitigate heat. This reflects social injustice where vulnerable populations often lack access to green infrastructures and could not even afford electricity prices of refrigeration equipment (Jenerette et al., 2011; Rocha et al., 2024). This finding suggests that targeted investments in green infrastructure should be made in these high-vulnerability areas to reduce their exposure to heat, named as priority areas in Fig. 3.

In dry climates like the Mediterranean, characterized by hot and dry summers, green cover becomes especially crucial for cooling (Grilo et al., 2020; Maggiotto et al., 2021). The significant role of the percentage of green cover in reducing heat is well-documented, largely due to shading and evapotranspiration, which lowers surrounding air temperatures (Bowler et al., 2010; Zhou et al., 2017). The particular dry summer conditions of the Granada region make it necessary to rely on drought-resistant species to achieve sustainable cooling effects through green infrastructure. These species, typically well-adapted to seasonal

water shortages, particularly xerophytic species or deep-rooted trees, can maintain significant evapotranspiration rates helping reduce local temperatures without straining water resources, even in harsh, dry conditions (Shashua-Bar et al., 2004; Leotta et al., 2023). However, it was not only the green cover that played a major role in maximizing the cooling effects of vegetation, but also the combination of large patch areas. This insight could inform urban planners on how to optimize green infrastructure in cities to maximize heat mitigation (Li et al., 2013; Silveira et al., 2024). However, in densely populated and built-up areas, like Granada city or other Mediterranean cities, we suggest that interventions could be developed connecting green infrastructures thus increasing their green cover and patch area, and ultimately their cooling capacity (see also Kleerekoper et al., 2012; Ziter et al., 2019; Delgado-Capel et al., 2023; Jungman et al., 2023). Our findings underscore the need for city management strategies that prioritize heat-vulnerable populations while optimizing green infrastructure's spatial configuration by focusing on Nature-based Solutions.

5. Conclusion

This study highlights the intricate links between the urban heat island, social vulnerability, and green infrastructure, demonstrating that urban heat risk is influenced by both physical and social aspects. The InVEST Urban Cooling model proved to be a practical and reliable tool for mapping urban heat islands, quantifying cooling ecosystem services, and assessing heat stress at a scale relevant to urban management. By integrating heat indicators into our framework, we extend the methodological application of the model, effectively bridging ecosystem service assessments with human vulnerability analysis. In a Mediterranean city with serious environmental problems, such as Granada, green cover, when greater than 35 %, and mean patch size above 200 m², maximized heat mitigation indicating that both are determining factors to be considered in the design of Nature-based Solutions. However, planning green infrastructures must also consider social-economic aspects, such as age and poverty, so that their benefits reach the whole population. Our findings provide targeted areas for urban planning interventions that prioritize highly vulnerable and exposed populations to heat and recommendations to optimize the spatial configuration of green infrastructure for effective heat mitigation.

CRedit authorship contribution statement

Silveira Carson: Writing – review & editing, Writing – original draft, Visualization, Methodology, Formal analysis, Data curation, Conceptualization. **Pistón Nuria:** Writing – review & editing, Writing – original draft, Visualization, Supervision, Methodology, Formal analysis, Conceptualization. **Martínez-López Javier:** Writing – review & editing, Methodology, Data curation. **Alcaraz-Segura Domingo:** Writing – review & editing, Methodology, Funding acquisition. **Postma Thedmer:** Writing – review & editing, Data curation. **López-Torralbo Juan Manuel:** Writing – review & editing, Data curation. **Zamora Regino:** Writing – review & editing, Resources, Methodology, Funding acquisition.

Declaration of Competing Interest

The authors declare that they have no known competing financial interests or personal relationships that could have appeared to influence the work reported in this paper.

Acknowledgement

We thank José Carlos Pérez-Girón and Carlos Navarro for their support of geoprocessing in a previous version of this manuscript. CS was funded from the Thematic Center on Mountain Ecosystem & Remote sensing, Deep learning-AI e-Services University of Granada-Sierra

Nevada (Smart EcoMountains LifeWatch-2019–10-UGR-01) co-funded by the Ministry of Science and Innovation and the LifeWatch-ERIC action line; NP received funding from the Spanish Ministry of Universities and NextGenerationEU (Maria Zambrano fellowship) and the BioCiTrees project, financially supported by EU's Horizon 2020 (HORIZON-MSCA-2022-PF-01, Project n° 101105829). JML was funded by the Plan Propio de Investigación (P9) of the University of Granada. This work was funded by grants BIOD22_001 and BIOD22_002, funded by Consejería de Universidad, Investigación e Innovación and Gobierno de España and Unión Europea – NextGenerationEU. The LiDAR point cloud was provided by the Red de Información Ambiental de Andalucía (REDIAM) - Consejería de Sostenibilidad, Medio Ambiente y Economía Azul, Junta de Andalucía.

Appendix A. Supporting information

Supplementary data associated with this article can be found in the online version at [doi:10.1016/j.ufug.2025.128794](https://doi.org/10.1016/j.ufug.2025.128794).

References

- Agencia Estatal de Meteorología., 2023. Olas de calor en España desde 1975—Agencia Estatal de Meteorología—AEMET. Gobierno de España, https://www.aemet.es/es/conocermas/recursos_en_linea/publicaciones_y_estudios/estudios/detalles/olascalor.
- Aldrich, N., Benson, W.F., 2007. Disaster preparedness and the chronic disease needs of vulnerable older adults. *Prev. Chronic Dis.* 5 (1). A27.
- Allen, R.G., Pereira, L.S., Raes, D., Smith, M., 1998. *Crop Evapotranspiration: Guidelines for Computing Crop Water Requirements*. FAO Irrigation and Drainage Paper 56. FAO, Rome, p. 300.
- Arnfield, A.J., 2003. Two decades of urban climate research: a review of turbulence, exchanges of energy and water, and the urban heat island. *Int. J. Climatol.* 23 (1), 1–26. <https://doi.org/10.1002/joc.859>.
- Bosch, M., Locatelli, M., Hamel, P., Remme, R.P., Jaligot, R., Chenal, J., Joost, S., 2021. Evaluating urban greening scenarios for urban heat mitigation: a spatially explicit approach. *R. Soc. Open Sci.* 8, 202174. <https://doi.org/10.1098/rsos.202174>.
- Bowler, D.E., Buyung-Ali, L., Knight, T.M., Pullin, A.S., 2010. Urban greening to cool towns and cities: A systematic review of the empirical evidence. *Landsc. Urban Plan.* 97 (3), 147–155. <https://doi.org/10.1016/j.landurbplan.2010.05.006>.
- Chakraborty, T.C., Qian, Y., 2024. Urbanization exacerbates continental- to regional-scale warming. *One Earth* 7 (8), 1387–1401. <https://doi.org/10.1016/j.oneear.2024.05.005>.
- Chakraborty, T., Hsu, A., Manya, D., Sheriff, G., 2019. Disproportionately higher exposure to urban heat in lower-income neighborhoods: a multi-city perspective. *Environ. Res. Lett.* 14 (10), 105003. <https://doi.org/10.1088/1748-9326/ab3b99>.
- Chen, A., Yao, L., Sun, R., Chen, L., 2014a. How many metrics are required to identify the effects of the landscape pattern on land surface temperature? *Ecol. Indic.* 45, 424–433. <https://doi.org/10.1016/j.ecolind.2014.05.002>.
- Chen, A., Yao, X.A., Sun, R., Chen, L., 2014b. Effect of urban green patterns on surface urban cool islands and its seasonal variations. *Urban For. Urban Green.* 13 (4), 646–654. <https://doi.org/10.1016/j.ufug.2014.07.006>.
- Chen, M., Chen, L., Zhou, Y., Hu, M., Jiang, Y., Huang, D., Gong, Y., Xian, Y., 2023. Rising vulnerability of compound risk inequality to ageing and extreme heatwave exposure in global cities. *Npj Urban Sustain.* 3 (1), 1–11. <https://doi.org/10.1038/s42949-023-00118-9>.
- Coffel, E.D., Horton, R.M., Sherbinin, A. de, 2017. Temperature and humidity based projections of a rapid rise in global heat stress exposure during the 21st century. *Environ. Res. Lett.* 13 (1), 014001. <https://doi.org/10.1088/1748-9326/aaa00e>.
- Coutts, A.M., Harris, R.J., Phan, T., Livesley, S.J., Williams, N.S.G., Tapper, N.J., 2016. Thermal infrared remote sensing of urban heat: hotspots, vegetation, and an assessment of techniques for use in urban planning. *Remote Sens. Environ.* 186, 637–651. <https://doi.org/10.1016/j.rse.2016.09.007>.
- De Pauw, K., Depauw, L., Cousins, S.A.O., De Lombaerde, E., Diekmann, M., Frey, D., Kwietniowska, K., Lenoir, J., Meeussen, C., Orzechowska, A., Plue, J., Spicher, F., Vanneste, T., Zellweger, F., Verheyen, K., Vangansbeke, P., De Frenne, P., 2024. The urban heat island accelerates litter decomposition through microclimatic warming in temperate urban forests. *Urban Ecosyst.* 27 (3), 909–926. <https://doi.org/10.1007/s11252-023-01486-x>.
- Delgado-Capel, M., Cariñanos, P., 2020. Towards a Standard Framework to Identify Green Infrastructure Key Elements in Dense Mediterranean Cities. *Forests* 11 (12), 1246. <https://doi.org/10.3390/f11121246>.
- Delgado-Capel, M.J., Cariñanos, P., Escudero-Viñolo, M., 2023. Capacity of urban green infrastructure spaces to ameliorate heat wave impacts in mediterranean compact cities: case study of Granada (South-Eastern Spain). *Land* 12 (5), 1076. <https://doi.org/10.3390/land12051076>.
- Dong, J., Guo, R., Lin, M., Guo, F., Zheng, X., 2024. Multi-objective optimization of green roof spatial layout in high-density urban areas—a case study of Xiamen Island, China. *Sustain. Cities Soc.* 115, 105827. <https://doi.org/10.1016/j.scs.2024.105827>.

- Elith, J., Leathwick, J.R., Hastie, T., 2008. A working guide to boosted regression trees. *J. Anim. Ecol.* 77 (4), 802–813. <https://doi.org/10.1111/j.1365-2656.2008.01390.x>.
- ESPON Climate. (2022). Updating and integrating climate datasets and maps. Final report. TU Dortmund University, ESPON & IRPUD.
- Georgescu, M., Broadbent, A.M., Krayenhoff, E.S., 2024. Quantifying the decrease in heat exposure through adaptation and mitigation in twenty-first-century US cities. *Nat. Cities* 1 (1), 42–50. <https://doi.org/10.1038/s44284-023-00001-9>.
- Grilo, F., Pinho, P., Aleixo, C., Catita, C., Silva, P., Lopes, N., Freitas, C., Santos-Reis, M., McPhearson, T., Branquinho, C., 2020. Using green to cool the grey: modelling the cooling effect of green spaces with a high spatial resolution. *Sci. Total Environ.* 724, 138182. <https://doi.org/10.1016/j.scitotenv.2020.138182>.
- Grimmond, C.S., Oke, T.R., 1999. Evapotranspiration rates in urban areas. *IAHS Publ.* 259, 235–243.
- Haaland, C., van den Bosch, C.K., 2015. Challenges and strategies for urban green-space planning in cities undergoing densification: a review. *Urban For. Urban Green.* 14 (4), 760–771. <https://doi.org/10.1016/j.ufug.2015.07.009>.
- Hamel, P., Bosch, M., Tardieu, L., Lemonsu, A., de Munck, C., Nootenboom, C., Vigiú, V., Lonsdorf, E., Douglass, J.A., Sharp, R.P., 2024. Calibrating and validating the Integrated Valuation of Ecosystem Services and Tradeoffs (InVEST) urban cooling model: case studies in France and the United States. *Geosci. Model Dev.* 17 (12), 4755–4771. <https://doi.org/10.5194/gmd-17-4755-2024>.
- Hamel, P., Guerry, A.D., Polasky, S., Han, B., Douglass, J.A., Hamann, M., Janke, B., Kuiper, J.J., Levrel, H., Liu, H., Lonsdorf, E., McDonald, R.I., Nootenboom, C., Ouyang, Z., Remme, R.P., Sharp, R.P., Tardieu, L., Vigiú, V., Xu, D., Daily, G.C., 2021. Mapping the benefits of nature in cities with the InVEST software. *Npj Urban Sustain.* 1, 25. <https://doi.org/10.1038/s42949-021-00027-9>.
- Herreros-Cantis, P., Hoffman, L., Kennedy, C., Kim, Y., Charles, J., Gillet, V., Getzin, A., Littlefield, D., Zielinski, A., Bernstein, J., Settle-Robinson, R., Langemeyer, J., Neumann, M.B., McPhearson, T., 2024. Co-producing research and data visualization for environmental justice advocacy in climate change adaptation: the milwaukee flood-health vulnerability assessment. *Cities* 155, 105474. <https://doi.org/10.1016/j.cities.2024.105474>.
- Hess, J.J., Errett, N.A., McGregor, G., Busch Isaksen, T.M., Wettstein, Z.S., Wheat, S.K., Ebi, K.L., 2023. Public health preparedness for extreme heat events. *Annu. Rev. Public Health* 44, 301–321. <https://doi.org/10.1146/annurev-publhealth-071421-025508>.
- Hidalgo-García, D., Arco-Díaz, J., 2022. Modeling the Surface Urban Heat Island (SUHI) to study of its relationship with variations in the thermal field and with the indices of land use in the metropolitan area of Granada (Spain). *Sustain. Cities Soc.* 87, 104166. <https://doi.org/10.1016/j.scs.2022.104166>.
- Hijmans, R.J., Phillips, S., Leathwick, J., Elith, J., 2017. *dismo: species distribution modeling*. R. Package Version 1, 1–4.
- Hothorn, T., Bretz, F., Westfall, P., 2008. Simultaneous Inference in General Parametric Models. *Biometrical Journal* 50 (3), 346–363. <https://doi.org/10.1002/bimj.200810425>.
- Hsu, A., Sheriff, G., Chakraborty, T., Many, D., 2021. Disproportionate exposure to urban heat island intensity across major US cities. *Nat. Commun.* 12 (1), 2721. <https://doi.org/10.1038/s41467-021-22799-5>.
- Instituto de Estadística y Cartografía de Andalucía. (2020a). Sistema de Información Multiterritorial de Andalucía (SIMA) - Indicadores demográficos por secciones censales. (https://www.juntadeandalucia.es/institutodeestadisticaycartografia/badea/operaciones/consulta/anual/87170?CodOper=b3_151&codConsulta=87170).
- Instituto de Estadística y Cartografía de Andalucía. (2020b). Inventario de Sedes y Equipamientos de la Junta de Andalucía (ISE). (<https://www.juntadeandalucia.es/institutodeestadisticaycartografia/dega/inventario-de-sedes-y-equipamientos-de-la-junta-de-andalucia-ise>).
- Instituto Geográfico Nacional. (2023). Base Topográfica Nacional de España. (<https://centrodedescargas.cnig.es/CentroDescargas/btn>).
- Instituto Nacional de Estadística. (2020a). Resultados por municipios, distritos y secciones censales por provincias - Granada - Indicadores de renta media y mediana. (<https://www.ine.es/jaxiT3/Tabla.htm?t=31025&L=0>).
- Instituto Nacional de Estadística. (2020b). Resultados por municipios, distritos y secciones censales por provincias - Granada - Porcentaje de población con ingresos por unidad de consumo por debajo/en cima de determinados umbrales relativos por sexo. (<https://www.ine.es/jaxiT3/Tabla.htm?t=31030&L=0>).
- IPCC. (2012). Managing the Risks of Extreme Events and Disasters to Advance Climate Change Adaptation. A Special Report of Working Groups I and II of the Intergovernmental Panel on Climate Change [Field, C.B., Barros, V., Stocker, T.F., Qin, D., Dokken, D.J., Ebi, K.L., Mastrandrea, M.D., Mach, K.J., Plattner, G.-K., Allen, S.K., Tignor, M. & Midgley P.M. (eds.)]. Cambridge University Press, Cambridge, UK, and New York, NY, USA, 582 pp.
- Iungman, T., Cirach, M., Marando, F., Barboza, E.P., Khomenko, S., Masselot, P., Quijal-Zamorano, M., Mueller, N., Gasparini, A., Urquiza, J., Heris, M., Thondoo, M., Nieuwenhuijsen, M., 2023. Cooling cities through urban green infrastructure: a health impact assessment of European cities. *Lancet* 401 (10376), 577–589. [https://doi.org/10.1016/S0140-6736\(22\)02585-5](https://doi.org/10.1016/S0140-6736(22)02585-5).
- Jenerette, G.D., Harlan, S.L., Stefanov, W.L., Martin, C.A., 2011. Ecosystem services and urban heat riskscape moderation: water, green spaces, and social inequality in Phoenix, USA. *Ecol. Appl.* 21 (7), 2637–2651. <https://doi.org/10.1890/10.1493.1>.
- Jiao, M., Xue, H., Yan, J., Zheng, Z., Wang, J., Zhao, C., Zhang, L., Zhou, W., 2021. Tree abundance, diversity and their driving and indicative factors in Beijing's residential areas. *Ecol. Indic.* 125, 107462. <https://doi.org/10.1016/j.ecolind.2021.107462>.
- Kadaverugu, R., Gurav, C., Rai, A., Sharma, A., Matli, C., Biniwale, R., 2021. Quantification of heat mitigation by urban green spaces using InVEST model—a scenario analysis of Nagpur City, India. *Arab. J. Geosci.* 14 (2), 82. <https://doi.org/10.1007/s12517-020-06380-w>.
- Kleerekooper, L., van Esch, M., Salcedo, T.B., 2012. How to make a city climate-proof, addressing the urban heat island effect. *Resour., Conserv. Recycl.* 64, 30–38. <https://doi.org/10.1016/j.resconrec.2011.06.004>.
- Kong, F., Yin, H., Wang, C., Cavan, G., James, P., 2014. A satellite image-based analysis of factors contributing to the green-space cool island intensity on a city scale. *Urban For. Urban Green.* 13 (4), 846–853. <https://doi.org/10.1016/j.ufug.2014.09.009>.
- Leotta, L., Toscano, S., Romano, D., 2023. Which plant species for green roofs in the mediterranean environment. *Plants* 12 (23), 3985. <https://doi.org/10.3390/plants12233985>.
- Li, D., Bou-Zeid, E., 2013. Synergistic interactions between urban heat islands and heat waves: the impact in cities is larger than the sum of its parts. *J. Appl. Meteorol. Climatol.* 52 (9), 2051–2064. <https://doi.org/10.1175/JAMC-D-13-02.1>.
- Li, J., Song, C., Cao, L., Zhu, F., Meng, X., Wu, J., 2011. Impacts of landscape structure on surface urban heat islands: a case study of Shanghai, China. *Remote Sens. Environ.* 115 (12), 3249–3263. <https://doi.org/10.1016/j.rse.2011.07.008>.
- Li, X., Zhou, W., Ouyang, Z., 2013. Relationship between land surface temperature and spatial pattern of greenspace: What are the effects of spatial resolution? *Landscape Urban Plan.* 114, 1–8. <https://doi.org/10.1016/j.landurbplan.2013.02.005>.
- Liu, Z., Zhan, W., Bechtel, B., Voogt, J., Lai, J., Chakraborty, T., Wang, Z.-H., Li, M., Huang, F., Lee, X., 2022. Surface warming in global cities is substantially more rapid than in rural background areas. *Commun. Earth Environ.* 3 (1), 1–9. <https://doi.org/10.1038/s43247-022-00539-x>.
- Maggiotto, G., Miani, A., Rizzo, E., Castellone, M.D., Piscitelli, P., 2021. Heat waves and adaptation strategies in a mediterranean urban context. *Environ. Res.* 197, 111066. <https://doi.org/10.1016/j.envres.2021.111066>.
- Marando, F., Heris, M.P., Zulian, G., Udiás, A., Mentaschi, L., Chrysoulakis, N., Parastatidis, D., Maes, J., 2022. Urban heat island mitigation by green infrastructure in European Functional Urban Areas. *Sustain. Cities Soc.* 77, 103564. <https://doi.org/10.1016/j.scs.2021.103564>.
- Mashhoodi, B., Kasraian, D., 2024. Heatwave exposure inequality: An urban-rural comparison of environmental justice. *Appl. Geogr.* 164, 103216. <https://doi.org/10.1016/j.apgeog.2024.103216>.
- Massaro, E., Schifanello, R., Piccardo, M., Caporaso, L., Taubenböck, H., Cescatti, A., Duveiller, G., 2023. Spatially-optimized urban greening for reduction of population exposure to land surface temperature extremes. *Nat. Commun.* 14, 2903. <https://doi.org/10.1038/s41467-023-38596-1>.
- Hesselbarth, M.H.K., Sciaini, M., With, K.A., Wiegand, K., Nowosad, J., 2019. *landscapemetrics: an open-source R tool to calculate landscape metrics*. *Ecography* 42, 1648–1657.
- Mirzabaei, A.; Wu, J.; Evans, J.; Garcia-Oliva, F.; Hussein, I.A.G.; Iqbal, M.H.; Kimutai, J.; Knowles, T.; Meza, F.; Nedjrooui, D.; Tena, F.; Türkes, M.; Vázquez, R.J. & Weltz, M. (2019). Desertification. In P. R. Shukla, J. Skeg, E. Calvo Buendia, V. Masson-Delmotte, H.-O. Pörtner, D. C. Roberts, P. Zhai, R. Slade, S. Connors, S. van Diemen, M. Ferrat, E. Haughey, S. Luz, M. Pathak, J. Petzold, J. Portugal Pereira, P. Vyas, E. Huntley, K. Kissick, M. Belkacemi & J. Malley (eds.), *Climate Change and Land: an IPCC special report on climate change, desertification, land degradation, sustainable land management, food security, and greenhouse gas fluxes in terrestrial ecosystems*. Natural Capital Project InVEST 0.0 Chinese Academy of Sciences, The Nature Conservancy 2024 Stanford University, University. <https://naturalcapitalproject.stanford.edu/software/invest>.
- Oke, T.R., 1973. City size and the urban heat island. *Atmos. Environ.* (1967) 7 (8), 769–779. [https://doi.org/10.1016/0004-6981\(73\)90140-6](https://doi.org/10.1016/0004-6981(73)90140-6).
- Oppenheimer, M., Campos, M., Warren, R., Birkmann, J., Luber, G., O'Neill, B., Takahashi, K., 2014. Emergent risks and key vulnerabilities. In: Field, C.B., Barros, V. R., Dokken, D.J., Mach, K.J., Mastrandrea, M.D., Bilir, T.E., Chatterjee, M., Ebi, K.L., Estrada, Y.O., Genova, R.C., Girma, B., Kissel, E.S., Levy, A.N., MacCrack, S., Mastrandrea, P.R., White, L.L. (Eds.), *In: Climate Change 2014: Impacts, Adaptation, and Vulnerability. Part A: Global and Sectoral Aspects. Contribution of Working Group II to the Fifth Assessment Report of the Intergovernmental Panel on Climate Change*. Cambridge University Press, pp. 1039–1099.
- Prado, H.A., Rodrigues, T., Manes, S., Kasecker, T., Vale, M.M., Scarano, F.R., Pires, A.P. F., 2024. Designing nature to be a solution for climate change in cities: a meta-analysis. *Sci. Total Environ.* 954, 176735. <https://doi.org/10.1016/j.scitotenv.2024.176735>.
- Peng, S., Piao, S., Ciais, P., Friedlingstein, P., Otle, C., Bréon, F.-M., Nan, H., Zhou, L., Myrneni, R.B., 2012. Surface urban heat island across 419 global big cities. *Environ. Sci. Technol.* 46 (2), 696–703. <https://doi.org/10.1021/es2030438>.
- Perkins, S.E., Alexander, L.V., Nairn, J.R., 2012. Increasing frequency, intensity and duration of observed global heatwaves and warm spells. *Geophys. Res. Lett.* 39, L20714. <https://doi.org/10.1029/2012GL053361>.
- Phelan, P.E., Kaloush, K., Miner, M., Golden, J., Phelan, B., Iii, H.S., Taylor, R.A., 2015. Urban heat island: mechanisms, implications, and possible remedies. *Annu. Rev. Environ. Resour.* 40, 285–307. <https://doi.org/10.1146/annurev-environ-102014-021155>.
- Pistón, N., de Bello, F., Dias, A.T.C., Götzenberger, L., Rosado, B.H.P., de Mattos, E.A., Salguero-Gómez, R., Carmona, C.P., 2019. Multidimensional ecological analyses demonstrate how interactions between functional traits shape fitness and life history strategies. *J. Ecol.* 107 (5), 2317–2328. <https://doi.org/10.1111/1365-2745.13190>.
- Pistón, N., Silva Filho, D.S.E., Dias, A.T.C., 2022. Social inequality deeply affects people's perception of ecosystem services and disservices provided by street trees. *Ecosyst. Serv.* 58, 101480. <https://doi.org/10.1016/j.ecoser.2022.101480>.
- PNOA. (2020a). Plan Nacional de Ortofotografía Aérea. Instituto Geográfico Nacional. Ministerio de Transportes, Gobierno de España: Madrid, España. (<https://portalredia>

- m.cica.es/geonetwork/srv/api/records/cbd671486ddc0c9c23d35f63d2ad8515306f7415).
- PNOA, (2020b). Plan Nacional de Ortofotografía Aérea. Instituto Geográfico Nacional. Ministerio de Transportes, Gobierno de España: Madrid, España. (<https://centrodedescargas.cnig.es/CentroDescargas/buscaadorCatalogo.do?codFamilia=LIDAR>).
- Prosdoci, D., Klima, K., 2020. Health effects of heat vulnerability in Rio de Janeiro: A validation model for policy applications. *SN Appl. Sci.* 2 (12), 1948. <https://doi.org/10.1007/s42452-020-03750-7>.
- REDIAM, 2023a. Portal Ambiental de Andalucía. Consejería de Sostenibilidad, Medio Ambiente y Economía Azul de la Junta de Andalucía. (https://portalrediam.cica.es/descargas?path=%2F01_CARACTERIZACION_TERRITORIO%2F08_SIPNA%2FSI_PNA_Pub2023_01).
- REDIAM, 2023b. Portal Ambiental de Andalucía. Consejería de Sostenibilidad, Medio Ambiente y Economía Azul de la Junta de Andalucía. (https://portalrediam.cica.es/descargas?path=%2F04_RECURSOS_NATURALES%2F03_CLIMA%2F02_CARACTERIZACION_CLIMATICA%2F07_EVAPOTRANSPIRACION).
- Ren, Y., Lafortezza, R., Giannico, V., Sanesi, G., Zhang, X., Xu, C., 2023. The unrelenting global expansion of the urban heat island over the last century. *Sci. Total Environ.* 880, 163276. <https://doi.org/10.1016/j.scitotenv.2023.163276>.
- Rocha, A.D., Vulova, S., Förster, M., Gioli, B., Matthews, B., Helfter, C., Meier, F., Steeneveld, G.-J., Barlow, J.F., Järvi, L., Chrysoulakis, N., Nicolini, G., Kleinschmit, B., 2024. Unprivileged groups are less served by green cooling services in major European urban areas. *Nat. Cities* 1 (6), 424–435. <https://doi.org/10.1038/s44284-024-00077-x>.
- Romanello, M., Napoli, C. di, Green, C., Kennard, H., Lampard, P., Scamman, D., Walawender, M., Ali, Z., Ameli, N., Ayeb-Karlsson, S., Beggs, P.J., Belesova, K., Ford, L.B., Bowen, K., Cai, W., Callaghan, M., Campbell-Lendrum, D., Chambers, J., Cross, T.J., Costello, A., 2023. The 2023 report of the Lancet Countdown on health and climate change: The imperative for a health-centred response in a world facing irreversible harms. *Lancet* 402 (10419), 2346–2394. [https://doi.org/10.1016/S0140-6736\(23\)01859-7](https://doi.org/10.1016/S0140-6736(23)01859-7).
- Russo, E., Domeisen, D.I.V., 2023. Increasing intensity of extreme heatwaves: the crucial role of metrics. *Geophys. Res. Lett.* 50 (14), e2023GL103540. <https://doi.org/10.1029/2023GL103540>.
- Schwartz, J., 2005. Who is sensitive to extremes of temperature?: a case-only analysis. *Epidemiology* 16 (1), 67. <https://doi.org/10.1097/01.ede.0000147114.25957.71>.
- Shashua-Bar, L., Tzamer, Y., Hoffman, M.E., 2004. Thermal effects of building geometry and spacing on the urban canopy layer microclimate in a hot-humid climate in summer. *Int. J. Climatol.* 24 (13), 1729–1742. <https://doi.org/10.1002/joc.1092>.
- Shashua-Bar, L., Pearlmutter, D., Erell, E., 2011. The influence of trees and grass on outdoor thermal comfort in a hot-arid environment. *Int. J. Climatol.* 31 (10), 1498–1506. <https://doi.org/10.1002/joc.2177>.
- Silveira, C., Dias, A.T.C., Amaral, F.G., de Gois, G., Pistón, N., 2024. The importance of private gardens and their spatial composition and configuration to urban heat island mitigation. *Sustain. Cities Soc.* 112, 105589. <https://doi.org/10.1016/j.scs.2024.1055>.
- Silveira, C., Pistón, N., Martínez-López, J., Alcaraz-Segura, D., Postma, T., López-Torralbo, J.M., Zamora, R., 2025. Assessing the effects of vegetation spatial patterns on urban heat mitigation, heat exposure, and vulnerability [Data set]. Zenodo. <https://doi.org/10.5281/zenodo.14691462>.
- Taha, H., Akbari, H., Rosenfeld, A., Huang, J., 1988. Residential cooling loads and the urban heat island—The effects of albedo. *Build. Environ.* 23 (4), 271–283. [https://doi.org/10.1016/0360-1323\(88\)90033-9](https://doi.org/10.1016/0360-1323(88)90033-9).
- Tuholske, C., Caylor, K., Funk, C., Verdin, A., Sweeney, S., Grace, K., Peterson, P., Evans, T., 2021. Global urban population exposure to extreme heat. *Proc. Natl. Acad. Sci.* 118 (41), e2024792118. <https://doi.org/10.1073/pnas.2024792118>.
- Wang, J., McPhearson, T., Zhou, W., Cook, E.M., Herreros-Cantis, P., Liu, J., 2023. Comparing relationships between urban heat exposure, ecological structure, and socio-economic patterns in Beijing and New York City. *Landscape Urban Plan.* 235, 104750. <https://doi.org/10.1016/j.landurbplan.2023.104750>.
- Wang, X., Blanchet, F.G., Koper, N., 2014. Measuring habitat fragmentation: an evaluation of landscape pattern metrics. *Methods Ecol. Evol.* 5 (7), 634–646. <https://doi.org/10.1111/2041-210X.12198>.
- Ye, J., Yang, F., 2025. Towards multi-scale and context-specific heat health risk assessment - A systematic review. *Sustain. Cities Soc.* 119, 106102. <https://doi.org/10.1016/j.scs.2024.106102>.
- Zardo, L., Geneletti, D., Pérez-Soba, M., Van Eupen, M., 2017. Estimating the cooling capacity of green infrastructures to support urban planning. *Ecosyst. Serv.* 26, 225–235. <https://doi.org/10.1016/j.ecoser.2017.06.016>.
- Zawadzka, J., Corstanje, R., Harris, J., Truckell, L., 2020. Downscaling Landsat-8 land surface temperature maps in diverse urban landscapes using multivariate adaptive regression splines and very high resolution auxiliary data. *Int. J. Digit. Earth* 13 (8), 899–914. <https://doi.org/10.1080/17538947.2019.1593527>.
- Zawadzka, J.E., Harris, J.A., Corstanje, R., 2021. Assessment of heat mitigation capacity of urban greenspaces with the use of InVEST urban cooling model, verified with daytime land surface temperature data. *Landscape Urban Plan.* 214, 104163. <https://doi.org/10.1016/j.landurbplan.2021.104163>.
- Zhou, W., Huang, G., Cadenasso, M.L., 2011. Does spatial configuration matter? Understanding the effects of land cover pattern on land surface temperature in urban landscapes. *Landscape Urban Plan.* 102 (1), 54–63. <https://doi.org/10.1016/j.landurbplan.2011.03.009>.
- Zhou, W., Wang, J., Cadenasso, M.L., 2017. Effects of the spatial configuration of trees on urban heat mitigation: a comparative study. *Remote Sens. Environ.* 195, 1–12. <https://doi.org/10.1016/j.rse.2017.03.043>.
- Zhou, W., Huang, G., Pickett, S.T.A., Wang, J., Cadenasso, M.L., McPhearson, T., Grove, J.M., Wang, J., 2021. Urban tree canopy has greater cooling effects in socially vulnerable communities in the US. *One Earth* 4 (12), 1764–1775. <https://doi.org/10.1016/j.oneear.2021.11.010>.
- Zhou, S., Chen, F., Xu, Z., 2022. Evaluating the accessibility of urban parks and waterfronts through online map services: A case study of Shaoxing, China. *Urban For. Urban Green.* 77, 127731. <https://doi.org/10.1016/j.ufug.2022.127731>.
- Ziter, C.D., Pedersen, E.J., Kucharik, C.J., Turner, M.G., 2019. Scale-dependent interactions between tree canopy cover and impervious surfaces reduce daytime urban heat during summer. *Proc. Natl. Acad. Sci.* 116 (15), 7575–7580. <https://doi.org/10.1073/pnas.181756111>.